J Mater Sci (2007) 42:10275–10283
DOI 10.1007/s10853-006-1122-4

Impedance spectroscopy and conductivity studies on B site modified $(Na_{0.5}Bi_{0.5})(Nd_xTi_{1-2x}Nb_x)O_3$ ceramics

Syed Mahboob · G. Prasad · Gobburu S. Kumar

Received: 8 November 2005 / Accepted: 10 October 2006 / Published online: 5 September 2007

Abstract Nd and Nb doped sodium bismuth titanate ceramics have been synthesized and characterized. Structural properties were obtained based on the XRD pattern analysis, indicating rhombohedral symmetry at room temperature. Impedance and conductivity (DC and AC) studies were done on polycrystalline samples. The results indicate that DC and AC conduction occurs by different mechanism in each case. The possible mechanism in the present case is discussed.

Introduction

Perovskite type ABO_3 disordered oxides with multiple ions occupying the lattice sites A and B have attracted considerable attention due to their dielectric relaxor, ferroelectric, semiconducting and electromechanical behaviour. The presence of heterovalent ions at lattice sites having different ionic radii, valence states and also varying polarizabilities has affected the dielectric, electrical and electromechanical properties.

$Na_{0.5}Bi_{0.5}TiO_3$ is one of the perovskite compounds that is extensively studied. Smolenskii et al., have first reported ferroelectricity in sodium bismuth titanate [1]. Sodium bismuth titanate is a very promising material for application point of view because of its strong ferroelectricity with a relatively large remanant polarization, $P_r = 38\ \mu C/cm^2$. This compound has a perovskite (ABO_3) structure with rhombohedral symmetry at room temperature and below 200 °C. It is reported that $Na_{0.5}Bi_{0.5}TiO_3$ has rhombohedral symmetry at room temperature. It undergoes a series of phase transitions: (i) ferroelectric rhombohedral to antiferroelectric tetragonal around 230 °C (503 K), (ii) antiferroelectric tetragonal to non-polar tetragonal around 320 °C (593 K) and finally (iii) non-polar tetragonal to cubic around 520 °C (793 K) [2]. The dielectric maximum occurs around 320 °C (593 K). Appropriate cationic modification at A site with (Pb, Sr, Pb + Sr, K etc) has resulted in good dielectric relaxor behaviour [3–8]. Dielectric studies on lanthanum doped sodium bismuth titanate ceramics by Aparna [9] revealed interesting changes in the dielectric and electromechanical properties. Lanthanum doping has broadened the dielectric peak showing diffusiveness of the phase transition. Lanthanum doped NBT sample ($Na_{1/2}La_{x/2}Bi_{(1-x)/2}TiO_3$) showed higher value of electromechanical coupling factor (K_{33}) of about 0.85 for $x = 0$ and 0.68 for $x = 0.1$ concentration. Sample with $x = 0.2$ showed higher value of room temperature pyroelectric coefficient ($p_{rt} = 176 \times 10^{-11}$ (C/cm^2 K)) when compared to sample with $x = 0.1$($p_{rt} = 3.5 \times 10^{-11}$ (C/cm^2 K)) and $x = 0.015$ ($p_{rt} = 1.7 \times 10^{-11}$ (C/cm^2 K)). It is well known that homo or heterovalent substitution at lattice sites A or B or both in ABO_3 type materials results in interesting dielectric relaxor, electrical conduction and electromechanical behaviour. This prompted the author to look into the effect of multiple heterovalent ions (Nd^{3+} and Nb^{5+}) doping at Ti^{4+} position in $Na_{0.5}Bi_{0.5}TiO_3$. In our earlier studies, we investigated the dielectric relaxor, electromechanical and ferroelectric properties of Nd and Nb doped $Na_{0.5}Bi_{0.5}TiO_3$ ceramics [10]. Hence, the results of impedance and conductivity (DC and AC) studies on polycrystalline $(Na_{0.5}Bi_{0.5})(Nd_xTi_{1-2x}Nb_x)O_3$ ceramics with $x = 0.0125$, 0.025 and 0.05 are presented in this paper.

S. Mahboob · G. Prasad · G. S. Kumar (✉)
Materials Research Laboratory, Department of Physics, Osmania University, Hyderabad 500 007 Andhra Pradesh, India
e-mail: gskumar1948@sify.com

Experimental procedure

$(Na_{0.5}Bi_{0.5})(Nd_xTi_{1-2x}Nb_x)O_3$ ceramics were prepared by solid-state synthesis using high purity (>99%) chemical reagents Na_2CO_3 (Aldrich), Bi_2O_3 (High media chemicals), Nd_2O_3 (Rare earths India Pvt. Ltd.), TiO_2 (Aldrich) and Nb_2O_5 (Nuclear Fuel Complex). Calcination for 15 h at 800 °C was followed by 4 h sintering at 1150 °C for $x = 0.0125$ and 0.025 and at 1125 °C for $x = 0.05$. The crystal structure and single phase formation was checked by X-ray powder diffractometer (Philips X-pert Pro Pan Analytical: Model PW3040/60). The microstructure of the sintered samples was taken on the fractured surface of the sample using SEM model LEICA S430. Impedance and AC conductivity data were obtained as a function of temperature (in the range 300–900 K) and frequency (in the range 800 Hz–1 MHz) using AUTOLAB low frequency impedance analyzer. DC conductivity was obtained through resistivity measurements using Keithley 617 programmable electrometer.

Results and discussion

Figure 1 shows the XRD pattern for $(Na_{0.5}Bi_{0.5})(Nd_xTi_{1-2x}Nb_x)O_3$ ceramics. The maximum intensity peak is observed around 32°, which is the characteristic feature of the present class of compounds. XRD pattern of the ceramic with the composition $x = 0.05$ has shown an extra peak around the main peak (32°), indicating a possible presence of some unidentifiable extra phase due to non-miscibility of substituted ions with the host lattice ion. All the peaks could be indexed based on the perovskite structure with rhombohedral symmetry. Lattice parameters were evaluated using XLAT. No systematic change in lattice parameter (a) was observed. However increase in α value with the increase of Nd and Nb concentration was observed (Table 1). This indicates that lattice distortion (90°-α) decreases with the increase of Nd and Nb concentration. This decrease in rhombohedral lattice distortion is attributed to the increase in average ionic radius of B site cations due to partial replacement of smaller Ti^{4+} ion (74 pm) with the larger ions

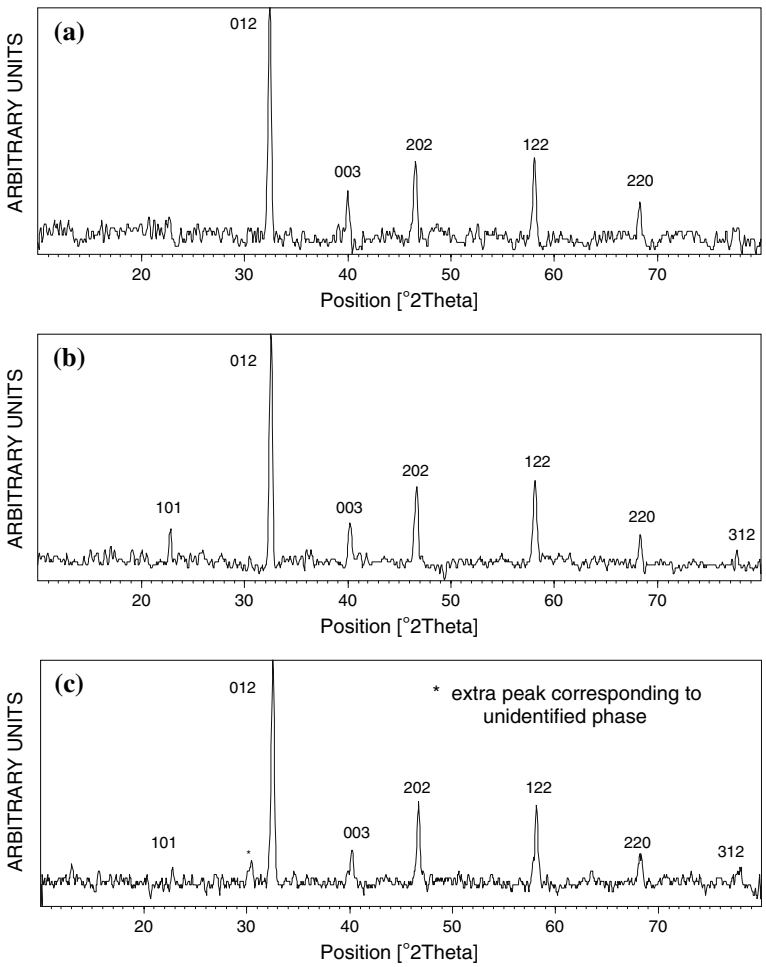

Fig. 1 XRD pattern of $(Na_{0.5}Bi_{0.5})(Nd_xTi_{1-2x}Nb_x)O_3$ samples for (**a**) $x = 0.0125$, (**b**) $x = 0.025$ and (**c**) $x = 0.05$

Table 1 Lattice parameters and density

Compound $[Na_{0.5}Bi_{0.5}][Nd_xTi_{1-2x}Nb_x]O_3$, $x = 0.0125$ (N1), $x = 0.025$ (N2), $x = 0.05$ (N3)	Lattice parameter		Density (gm/cm^3)		% Density
	a(A°)	A°	Theoretical	Experimental	
$[Na_{0.5}Bi_{0.5}]TiO_3$(Guo (1982))	3.886	89.600	5.99	–	–
N1	3.857	89.906	6.18	5.36	86.7
N2	3.895	89.908	6.05	5.57	92.1
N3	3.882	89.950	6.22	5.69	91.6

Nd^{3+} (112.3 pm) and Nb^{5+} (78 pm) causing smaller distortion of BO_6 octahedra. The experimental density of the samples is 86.7%, 92.1% and 91.6% of the theoretical X-ray density for $x = 0.0125$, 0.025 and 0.05 samples respectively. Figure 2 shows the scanning electron micrographs (SEM) for all compositions. These SEM graphs reflect the uniform grain distribution and have uniform grain size. The average grain size of the ceramic samples is about 1 μm (Fig. 2).

Figure 3 shows the variation of real and imaginary part of impedance (Z', Z'') with temperature at different frequencies for ceramic composition $x = 0.0125$. It can be observed from Fig. 3a that the value of Z' at low frequencies decreases gradually with the increase of temperature from 300 K to 600 K. Beyond 600 K a gradual increase in Z' value with increase of temperature was observed and Z' value reaches a maxima at a certain temperature (in the range 798–898 K) depending up on the frequency and thereafter drastic decrease in Z' value was observed with further increase of temperature. These Z' peaks at certain temperature are found to be frequency dependent and are shifting towards higher temperature side with increase of frequency indicating relaxation behaviour.

Figure 3b shows the thermal variation of Z'' values at different frequencies. Z'' value at lower frequencies is found to decrease with the increase of temperature from 300 K to 600 K. Beyond 600 K, Z'' value gradually increases with rise of temperature and in the temperature range 748–898 K a hump was observed. The temperature at which a hump was observed is found to be frequency dependent and found to be shifting towards higher temperature side with the increase of frequency indicating relaxation behaviour. For frequencies greater than 24.2 KHz, Z'' value remains almost constant in the investigated temperature range (300–898 K) and all the curves at different frequencies appear to merge in to a single value at higher temperatures.

Figure 4a–c shows Cole–Cole plots obtained for all compositions at 848 K. Equivalent circuit modelling was done to resolve the grain and grain boundary and electrode effects. The impedance data at 848 K for $x = 0.0125$, 0.025 was found to fit to series array of two sub circuits (each sub circuit consists of parallel RC combination) in series with a resistor, one corresponding to grain and other corresponding to grain boundary. The impedance data for $x = 0.05$ at 848 K was found to fit to series array of three sub circuits in series a resistor. The third RC circuit corresponds to

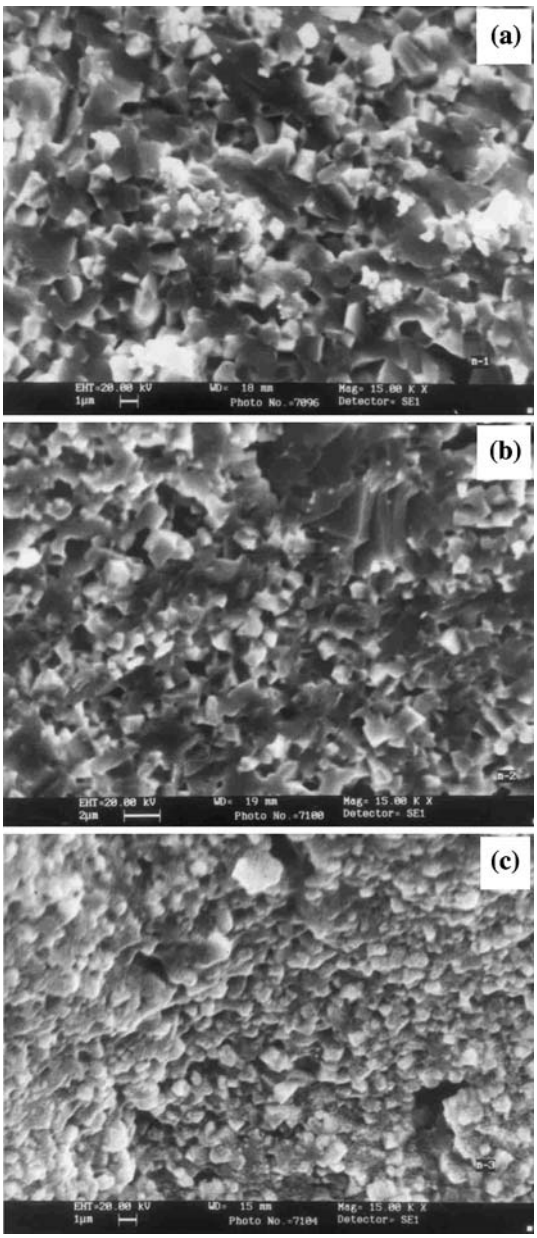

Fig. 2 SEM graphs of $(Na_{0.5}Bi_{0.5})(Nd_xTi_{1-2x}Nb_x)O_3$ samples for (**a**) $x = 0.0125$, (**b**) $x = 0.025$ and (**c**) $x = 0.05$

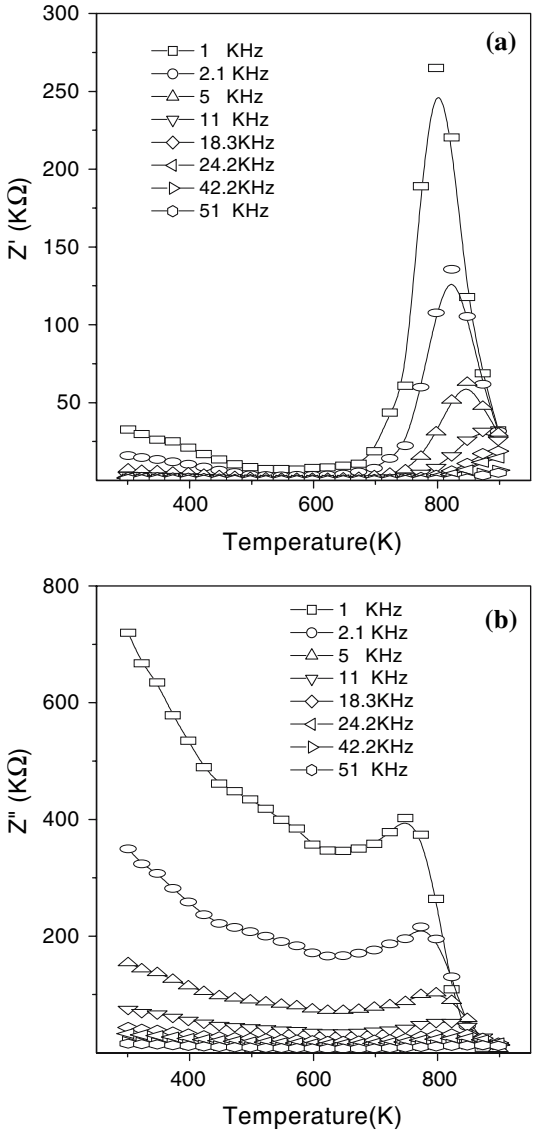

Fig. 3 (**a**) Z' vs. temperature (**b**) Z'' vs. temperature for $(Na_{0.5}Bi_{0.5})(Nd_xTi_{1-2x}Nb_x)O_3$ ceramic with $x = 0.0125$

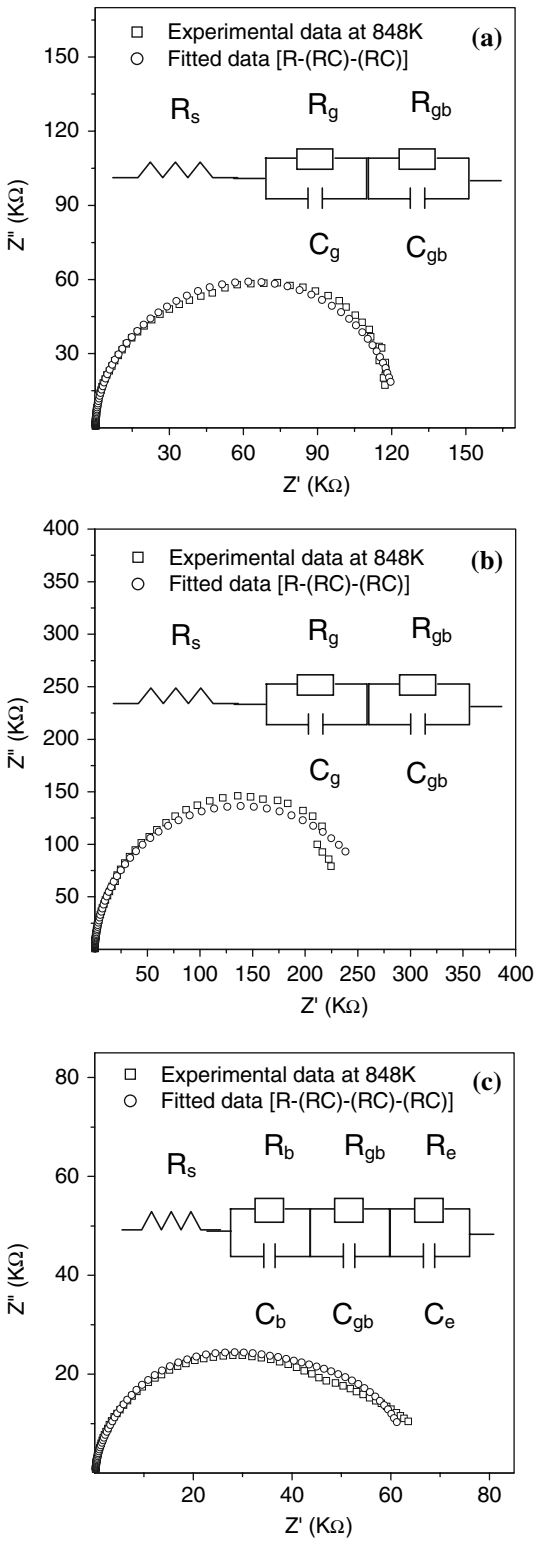

Fig. 4 Z'' vs. Z' plots of $(Na_{0.5}Bi_{0.5})(Nd_xTi_{1-2x}Nb_x)O_3$ ceramics with (**a**) $x = 0.0125$, (**b**) $x = 0.025$ and (**c**) $x = 0.05$

electrode effect**.** *The fitted parameter values at 848 K are shown in* Table 2. The data on grain, grain boundary resistance and relaxation frequency as a function of temperature (1,000/T) are presented in Fig. 5. The values of activation energy obtained from the Arrhenius plots of grain, grain boundary resistance and relaxation frequency are summarized in Table 3.

From DC conductivity studies, it was observed that the room temperature conductivity for all samples is of the order of 10^{-10} $(\Omega\ \text{cm})^{-1}$. Figure 6a shows $\log(\sigma_{dc})$ vs. 1,000/T(K) for all composition. In the measured temperature range the DC conductivity of all the samples is found vary by six to seven orders of magnitude. However it is observed that the conductivity value of $x = 0.0125$ sample steeply rises with temperature in range 575–660 K when compared to $x = 0.025$ and 0.05 sample. For all the samples a change in slope was observed at different temperature regions. Slope change in all the samples was observed

Table 2 Fitted parameters at 848 K

Sample	Fitted parameters at 848 K						
	R_s (Ω)	R_g (Ω)	C_g (F)	R_{gb} (Ω)	C_{gb} (F)	R_e (Ω)	C_e (F)
N1	163.4	11,150	1.03×10^{-9}	1,11,100	3.07×10^{-10}	–	–
N2	133.8	2,681	2.78 × E–9	2,72,300	2.72×10^{-10}	–	–
N3	196.1	2,344	9.48 × E–10	37,400	3.31×10^{-10}	24,100	2.50×10^{-9}

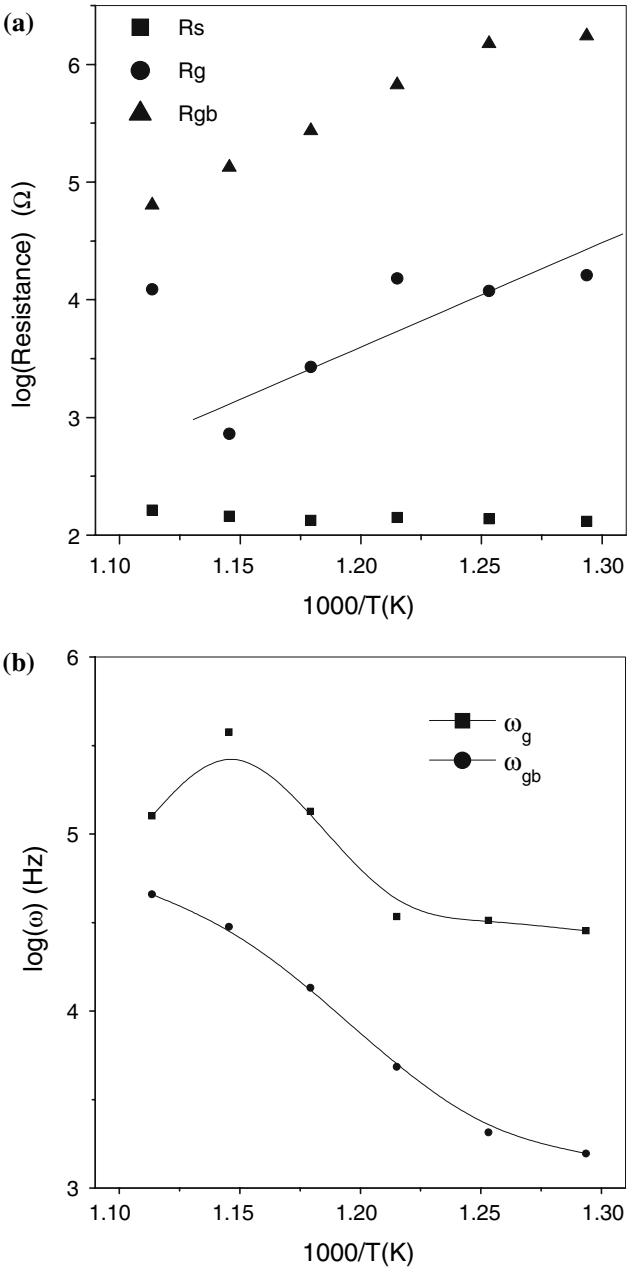

Fig. 5 (**a**) Log(resistance) vs. 1,000/T and (**b**) log(ω) vs. 1,000/T for $(Na_{0.5}Bi_{0.5})(Nd_xTi_{1-2x}Nb_x)O_3$ ceramic with $x = 0.025$

around the temperatures corresponding to the two dielectric anomalies in the temperature dependent dielectric plots. The slope changes at temperatures other than the temperatures corresponding to the dielectric anomalies may be attributed to change in conduction mechanism.

The Activation energy for DC conductivity (E_{dc}) in different temperature regions was obtained by fitting the conductivity data to the Arrhenius relation,

$$\sigma = \sigma_0 \exp(-E_{dc}/k_B T) \quad (1)$$

where σ_0 represents a pre-exponential factor and E, k_B and T are the apparent activation energy for DC conduction, Boltzmann's constant and the absolute temperature respectively. The E_{dc} values for all the samples are summarized in Table 4.

Figure 6b shows the AC conductivity plots as a function of 1,000/T at 11.5 KHz. It can be seen from these plots that in the measured temperature range (470–890 K), the AC conductivity at a lower frequency changes by two to three orders of magnitude. The activation energy for AC conductivity at different temperature regions obtained from the AC conductivity plots showing Arrhenius behaviour

$$\sigma'_{ac} = \sigma_0 \exp(-E_{ac}/k_B T) \quad (2)$$

and are summarized in Table 4, where E_{ac} the apparent activation energy for AC conduction.

The frequency dependent conductivity plots at different temperature regions for $x = 0.0125$ sample are shown in Fig. 7. It is observed that in the measured frequency range (800–1 MHz) and temperature range (300–900 K) AC conductivity changes by about one to four orders of magnitude. The data shows two slopes in the investigated frequency range (700 Hz to 1 MHz), one in the low frequency region and other in the higher frequency region. Similar behaviour was observed for other samples. Hence the two term power relation

$$\sigma'_{ac} = B_1 \omega^{s_1} + B_2 \omega^{s} 2 \quad (3)$$

is used to characterize the frequency dependence of AC conductivity. To extract more information regarding the mechanism of AC conductivity, the parameters (s_1, s_2) are obtained and are summarized in Table 5. Here s_1 is the low frequency range exponent and s_2 is the high frequency range exponent [11]).

In the present samples heterovalent ions (Nd^{3+} and Nb^{5+}) partially replaces the Ti^{4+} ions at B site and also

Table 3 Grain, grain boundary and sample-electrode interface activation energy and pre-exponential relaxation frequency values

Sample	Temperature range 798–873 K					
	Grain conduction activation energy (eV)			Grain relaxation activation energy (eV)		
	E_g	E_{gb}	E_e	ε_g	ε_{gb}	ε_e
N1	0.81	2.48	–	0.66	1.33	–
N2	2.41	1.96	–	2.08	2.18	–
N3	1.52	1.03	2.36	0.68	0.97	1.23

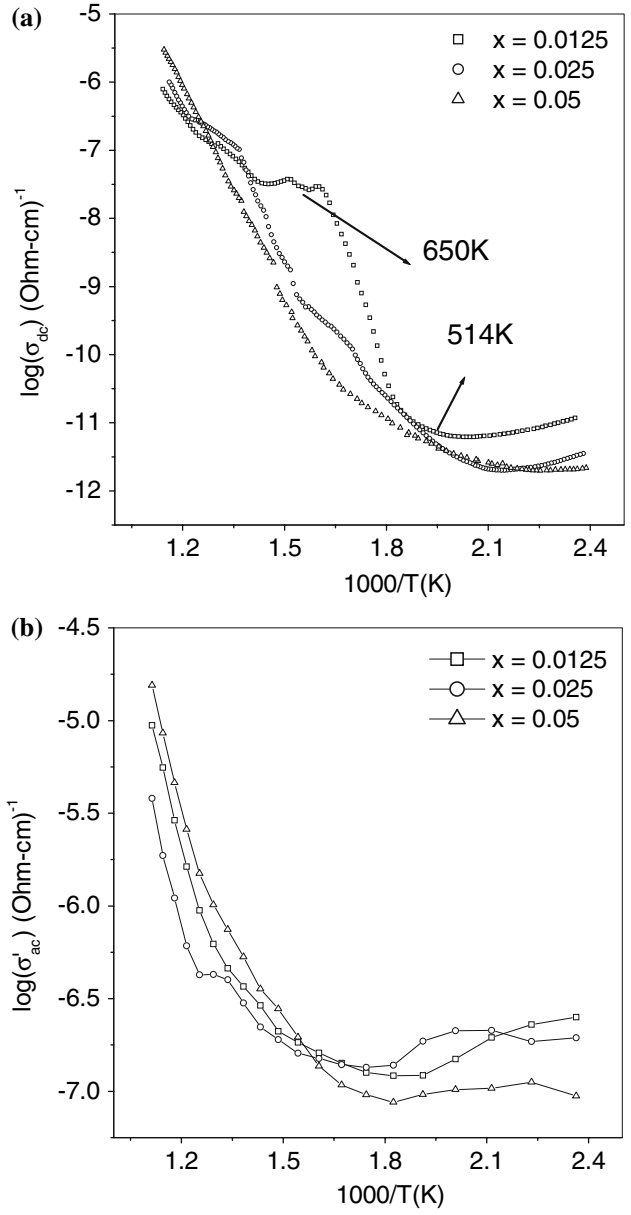

Fig. 6 (**a**) Log(σ_{dc}) vs. 1,000/T and (**b**) log(σ'_{ac}) vs. 1,000/T at 11.5 kHz of $(Na_{0.5}Bi_{0.5})(Nd_xTi_{1-2x}Nb_x)O_3$ ceramics

heterovalent ions (Na^{1+} and Bi^{3+}) occupy the lattice site A. There results localized oxygen, titanium and A site vacancies due to different valence states of the substituted ions when compared to host ions at A and B sites and the possible mechanism for the formation of these vacancies are illustrated in the following relations:

$$AO + TiO_2 \rightarrow A + Ti + 3O(ATiO_3) \quad (4)$$

(A represents divalent cation at A-site)

$$6AO + 3Nd_2O_3 \rightarrow 6A + 6Nd_{Ti} + 15O + 3V_O \quad (5)$$

$$5AO + 2Nb_2O_5 \rightarrow 5A + 4Nb_{Ti} + 15O + V_{Ti} \quad (6)$$

$$Bi_2O_3 + 3TiO_2 \rightarrow 2Bi_A + 3Ti + 9O + V_A \quad (7)$$

$$3Na_2O + 6TiO_2 \rightarrow 6Na_A + 6Ti + 15O + 3V_O \quad (8)$$

or

$$12AO + 10TiO_2 + 3Nd_2O_3 + 2Nb_2O_5 + Bi_2O_3 + 3Na_2O \rightarrow 12A + 10Ti + 6Nd_{Ti} + 4Nb_{Ti} + 2Bi_A + 6Na_A + V_A + V_{Ti} + 6V_O + 57O \quad (9)$$

where Nd_{Ti} represents the incorporation of Nd at Ti position, Nb_{Ti} represents the incorporation of Nb at Ti position, Na_A represents incorporation of Na at A site, Bi_A represents incorporation of Bi at A site position, V_{Ti} represents the titanium vacancy (with four effective positive charges), V_A represents the A site vacancy (with two effective positive charges), O represents the oxygen ion and V_O represents the oxygen vacancy (with two effective negative charges).

It is reported that a band gap of 3.5–4 eV exists between the O (2p) valence band and the Ti (3d) conduction band and a thermal energy of approximately 2 eV can transfer the electrons from the valence band to the conduction band leading to conductivity in Ti based oxide materials [12].

The activation energies for conductivity greater than or close to 2 eV in the present samples, indicates that the conduction across the grain boundary layer and conduction with in the grain in $x = 0.025$ sample arises due to the transfer of 3d electrons of Ti ions to the conduction band. Similarly the activation energy of about 2.48 eV across the

Table 4 Activation energy values for DC and AC conductivity

Sample	DC Conductivity activation energy (eV)			AC Conductivity activation energy (eV)					
				11.5 KHz			18.3 KHz		
	Temperature range (K)			Temperature range (K)			Temperature range (K)		
	540–600	700–770	800–885	540–600	700–770	800–885	540–600	700–770	800–885
N1	3.25	0.95	1.24	0.12	0.36	1.43	0.14	0.34	1.35
N2	1.26	2.04	1.37	0.03	0.53	1.36	0.05	0.44	1.25
N3	0.69	1.94	1.99	0.12	0.66	1.45	0.06	0.52	1.36

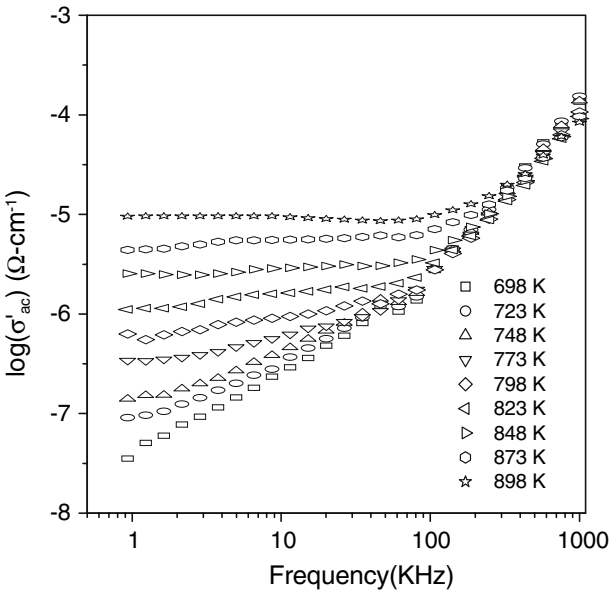

Fig. 7 Log(σ') vs. frequency for $(Na_{0.5}Bi_{0.5})(Nd_xTi_{1-2x}Nb_x)O_3$ ceramic with $x = 0.0125$

grain boundary layer in $x = 0.0125$ sample indicates similar phenomenon as mentioned above. There is also possibility that thermal fluctuation may liberate holes from the titanium vacancies (as illustrated in the relation given below), which in turn leads to activation energies for conductivity greater than or close to 2 eV.

$$V_{Ti} \rightarrow V_{Ti}'''' + 4h \quad (10)$$

(V_{Ti}'''' represents the titanium vacancy with zero effective positive charge and 'h' represents hole).

Oxygen vacancies present in the samples dissociate in to single and double ionized oxygen vacancies (V_O' and V_O'') liberating electrons when heated at high temperatures [13]. Ti^{4+} and Nb^{5+} ions in the present perovskite material capture these electrons to form Ti^{3+} and Nb^{3+}. The hopping of electrons between (Ti^{4+}–Ti^{3+}) and between (Nb^{5+}–Nb^{3+}) also contributes to the over all conductivity in the sample. There is a possibility of Ti^{3+} ion combining with singly ionized oxygen vacancy (Ti^{3+}-V_O') and Nb^{3+} ion to combine with oxygen vacancy (Nb^{3+}-V_O) to form dipoles. The response of such dipoles to temperature and frequency is attributed to the observed impedance relaxation behaviour as shown in Fig. 3a,b.

The activation energy for conductivity close to 1 eV is attributed to the oxygen vacancies related phenomenon. The low values of activation energy for relaxation (ε_g ε_{gb}) compared to activation energy for conduction (E_g, E_{gb}) for $x = 0.0125$ sample indicates that relaxation mechanism in the present samples occurs via (Ti^{3+}-V_O') and (Nb^{3+}-V_O)

Table 5 AC conductivity parameters

Temperature (K)	AC Parameters					
	$x = 0.0125$		$x = 0.025$		$x = 0.05$	
	s_1	s_2	s_1	s_2	s_1	s_2
673	0.78	1.87	0.82	1.94	0.55	1.81
723	0.53	1.86	0.41	1.87	0.45	1.80
748	0.46	1.83	0.32	1.86	0.45	1.71
798	0.22	1.76	0.30	1.83	0.25	1.58
823	0.17	1.69	0.21	1.82	0.20	1.45
848	0.03	1.58	0.11	1.70	0.13	1.13
873	0.02	1.40	0.01	1.65	0.05	1.13
898	0.01	1.20	0.01	1.46	0.03	0.85

dipoles (Tables 2 and 3). Similarly the low values of activation energy for relaxation (ε_g, ε_{gb} and ε_{gb}) when compared to activation energy for conduction (E_g, E_{gb} and E_e) for $x = 0.05$ sample are attributed to the relaxation of such dipoles. But in the case of $x = 0.025$ samples the activation energy for relaxation (ε_g and ε_{gb}) are found to be greater than 2 eV indicating relaxation of charged defects (i.e. titanium vacancies).

It is well known that the activation energy for relaxation of charged defects across the grain boundary layer and sample-electrode interface regions in disordered perovskite materials is fairly higher when compared to the grain relaxation energy. Perovskite type disordered materials contain long and short-range coulombic interactions, which in turn depends upon the degree of disorder. Usually in the grain boundary layer, the degree of ionic disorder is more when compared to ionic disorder in grains. The highly disordered ionic arrangements in the boundary layer causes very irregular coulombic potential fields, which discourage the migration of charged species as well as the reorientation of dipoles across the grain boundary layers. This must be the main reason for the higher values of observed activation energy of charged defects via dipole formation across the grain boundary layer for all samples as summarized in Tables 2 and 3).

The activation energy for DC conduction in different temperature regions for a given sample indicates that different conducting species are contributing to the conductivity in different temperature regions (Table 4). Change in activation energy is also observed around dielectric maximum temperatures. It is also observed that the activation energy for DC conductivity for $x = 0.0125$ sample in the low temperature region 540–600 K is 3.25 eV. Similar high values of activation energy for conduction was observed in the temperature region 700–770 K for $x = 0.025$ sample and in the temperature regions 700–885 K for $x = 0.05$ sample as shown in Table 4. This indicates that the conductivity in those temperature regions is predominately due to transfer of 3d electrons of Ti ions from valence band to the conduction band and also due to liberation of holes from the titanium vacancy as discussed in the previous paragraphs.

A large difference in the activation energy for DC conduction and AC conduction (at 11.5 KHz and 18.3 KHz) was observed at lower temperature regions and the activation energy for AC conduction is very small when compared to DC conduction (Table 4). This is expected because at lower temperature regions the DC conductivity is due to the mobility/transportation of conducting species over a long distance rather than reorientational mechanism as in AC conductivity via dipole formation ((Ti^{3+}-V_O') and (Nb^{3+}-V_O)). Thus the energy required in the latter case is very low when compared to former case. In the higher temperature region (880–885 K), a little variation in activation energy for DC and AC conduction (at 11.5 KHz and 18.3 KHz) was observed for all samples except for $x = 0.05$ sample. This indicates that the conductivity in higher temperature region in $x = 0.0125$ and 0.025 samples arises due to intrinsic property of the material.

It is well know that thermal fluctuation causes irregular scattering of the conducting species and also hinders the conductivity arising due to the reorientation mechanism. Hence if the thermal fluctuations are more, the more is the energy required for migration of charged species and conduction via reorientational mechanism. This is in good agreement with the results obtained which shows an increase in activation energy for AC conduction with the increase of temperature (Table 4).

From Table 5, it is observed that the value of s_2 at low temperatures (673 K) is around 2 and decreases gradually approaching 1 at higher temperatures. Similarly it is observed that the values of s_1 at low temperature (673 K) is around 0.7 and with the increase of temperature the value of s_1 gradually decreases approaching zero value at higher temperatures. Similar behaviour was observed for other samples as shown in Table 5. It was also observed for all samples that the value of s_1 lies between zero and one and the value of s_2 between zero and two. The value of s_2 (high frequency exponent) is always larger than s_1 (low frequency exponent).

As in the case of ionic crystals, in the perovskite ceramic materials there is a possibility of schottky and frenkel defects. The ions may move between lattice points (i.e. interstitial points for frenkel defects) and also by jumping over unoccupied points (for schottky defects). Movement of lattice ions at higher temperature may also lead to conductivity in the present samples. Hence, the AC conductivity data is interpreted in terms of jump relaxation model introduced by Funke [14] and also by the temperature dependence of exponents. The conduction in the low frequency region is associated with the short range translational hopping mechanism for $0<s_1<1$ and the conductivity in the higher frequency region is associated with the reorientational hopping mechanism for $0<s_2<2$. The short-range conduction in the samples occurs via hopping of 3d and 4d electrons between (Ti^{4+}–Ti^{3+}) and between (Nb^{5+}–Nb^{3+}). The reorientational hopping conduction arises due to formation of polaronic dipoles ((Ti^{3+}-V_O') and (Nb^{3+}-V_O) and these dipoles change their orientation by hopping of electrons between metal ions and oxygen vacancies.

Conclusions

The $(Na_{0.5}Bi_{0.5})(Nd_xTi_{1-2x}Nb_x)O_3$ with ($x = 0.0125$, 0.025 and 0.05) formed in to single phase materials with rhombo-

hedral symmetry at room temperature except for $x = 0.05$, which shows an extra unidentified peak around two theta (30°). A slight change in lattice parameter (a) with the increase of x and a corresponding decrease in rhombohedral distortion was observed. DC and AC conductivity analysis revealed that conduction occurs by different mechanism in each case. High activation energies (greater than or equal to 2 eV) were attributed to the transfer the 3dTi electrons from the valence band to the conduction band and also to the dissociation of titanium vacancy to liberate holes. The conductivity in the higher frequency region is associated with the reorientational hopping mechanism due to formation of polaronic dipoles (Ti^{3+}-V_O') and (Nb^{3+}-V_O) for $0 < s_2 < 2$. The conductivity in the low frequency region is associated with the short range translational hopping mechanism via hopping of 3d and 4d electrons between (Ti^{4+}-Ti^{3+}) and between (Nb^{5+}-Nb^{3+}) for $0 < s_1 < 1$.

Acknowledgements The authors would like to thank DRDO, Delhi, India for the financial support for carrying out the present research work. One of the authors Mr. Syed Mahboob would like to thank Head Department of Physics, Osmania University for providing XRD facility and to the Head, Paleontology department, GSI, Hyderabad for extending the SEM facility.

References

1. Smolenskii GA, Isupov VA, Agranovskaya AI, Krainik NN (1961) Sov Phys Solid State 2:2651
2. Takenaka T, Sakata K, Toda K (1990) Ferroelectrics 106:375
3. Suchanicz J, Gavshin MG, Kudzin AYu (2001) J Mater Sci 36:1981
4. Said S,Mercurio J-P (2001) J Eur Ceram Soc 21:1333
5. Bahuguna Saradhi BV, Srinivas K, Prasad G, Suryanarayana SV, Bhimasankaram T (2003) Mater Sci Eng B 98:10
6. Wang XX, Kwok KW, Tang XG, Chan HLW, Choy CL (2004) Solid State Commun 129:319
7. Gomah-Petty J-R, Senda S, Marchet P, Mercurio J-P (2004) J Eur Ceram Soc 24:1165
8. Qu Y, Shan D, Song J (2005) Mater Sci Eng B 121:148
9. Aparna M (2003) Electromechanical and electrical characterization of doped perovskite ferroelectrics through impedance spectroscopy. Department of Physics Osmania University, Hyderabad
10. Syed Mahboob GP, Kumar GS (2005) Mod Phys Letts B (communicated)
11. Ahmed AAY (2002) Z Naturforch 57a:263
12. Moulson AJ, Herbert JM (1990) Electro ceramics materials properties and applications. Chapman & Hall, London, p 226
13. Kroger FA, Vink H (1956) J Solid State Phys 3:307
14. Funke K (1993) Prog Solid State Chem 22:111